Journal of Computational Physics **161,** 1–20 (2000)
doi:10.1006/jcph.2000.6425, available online at http://www.idealibrary.com on IDEAL®

Lattice Boltzmann Algorithm for Simulating Thermal Flow in Compressible Fluids

Bruce J. Palmer and David R. Rector

Environmental and Molecular Sciences Laboratory, Box 999, Pacific Northwest National Laboratory,[1]
Richland, Washington 99352

Received March 9, 1999

An algorithm has been developed for incorporating the effects of temperature into lattice Boltzmann simulations. Instead of modeling the internal energy as a moment of the distribution describing the flow of mass and momentum, the internal energy is modeled as a scalar field using a second distribution. The energy is then coupled to the density and momentum via the partition between moving and nonmoving particles in a conventional two-speed model. The algorithm is tested against a number of systems for which analytic results are available. These include nonuniform conductivity between two plates, entry length behavior for flow in a channel between two parallel plates, and critical Rayleigh number behavior in Rayleigh–Bénard convection. Quantitative agreement is found in all cases. © 2000 Academic Press

1. INTRODUCTION

Lattice Boltzmann algorithms have recently begun to receive considerable attention as an alternative to conventional computational fluid dynamics for simulating fluid flow in certain classes of problems. These algorithms are based on the idea of trying to model a fluid by simulating a discretized one-particle phase space distribution function similar to the one described by the traditional Boltzmann equation. Describing a one-particle distribution function at each point in space requires more information than just specifying the usual hydrodynamic fields. However, the ease of implementing boundary conditions for complex geometries makes lattice Boltzmann simulations attractive candidates for studying flow in porous media and the local nature of the algorithms allows them to be easily adapted to parallel architecture computers. Lattice Boltzmann simulations with good stability properties have been developed that can quantitatively reproduce isothermal incompressible Navier–Stokes flow [1, 2].

[1] Pacific Northwest National Laboratory is operated for the U.S. Department of Energy by Battelle Memorial Institute under Contract DE-AC06-76RLO 1830.

0021-9991/00 $35.00
Copyright © 2000 by Academic Press
All rights of reproduction in any form reserved.

There has also been a great deal of interest in developing algorithms that can model thermal transport in addition to mass flow, but incorporating the effects of temperature into lattice Boltzmann simulations has proven to be unexpectedly difficult. The most obvious approach, in analogy to the traditional Boltzmann equation, is to define the internal energy to be a moment of the lattice Boltzmann distribution. An algorithm of this type based on multiple lattice speeds has been described [3], but it has poor stability properties [4] and can only simulate one value of the Prandtl number Pr (the ratio of kinematic viscosity to thermal diffusivity). An additional problem is that it may not be possible to model systems with nonideal gas thermodynamics. This algorithm has been generalized, at least in two dimensions, so that arbitrary Prandtl numbers can be simulated [4–6]. A second approach to modeling thermal flow using lattice Boltzmann techniques treats temperature as a passive diffusing scalar [7, 8]. This has the advantage of simplicity and can easily handle an arbitrary value of the Prandtl number but it cannot be used, except in an *ad hoc* way, for systems where there are significant changes in fluid density with temperature. Very recently, a two-distribution algorithm has been proposed by He *et al.* [9] that is similar to the two-distribution approach outlined below. However, this model is limited to systems with ideal gas thermodynamics.

This paper will present a detailed derivation of a new lattice Boltzmann algorithm for simulating thermal transport in fluid systems [10]. Quantitative comparisons of lattice Boltzmann simulations with analytic results for several thermal flow problems are also presented. The internal energy of the system in this algorithm is described by a second distribution that models the energy as a conserved scalar quantity, similar to the density. The internal energy can then be coupled back to the velocity and momentum fields in a relatively straightforward way. The hydrodynamic equations generated by this model are very close to the standard hydrodynamic equations of continuum fluid dynamics in the absence of viscous dissipation, and the algorithm naturally incorporates the thermodynamic properties of the fluid. Simulations on several test systems give quantitative agreement with analytic results.

2. THERMAL LATTICE BOLTZMANN MODEL

Lattice Boltzmann simulations are an alternative to classical fluid dynamics that model fluid flow by simulating the behavior of the one-particle distribution function, instead of solving the usual continuum hydrodynamic equations for the conserved fields [11]. The original Boltzmann equation describes the behavior of the one-particle distribution function $f(\mathbf{r}, \mathbf{v}, t)$, where f represents the probability of finding a fluid particle at the point $\mathbf{r}$ at time t, moving with velocity $\mathbf{v}$. If this function is known, then local values of the density, momentum, and temperature can be found by evaluating moments of f and these can be used to reconstruct any other local thermodynamic properties through the equation of state. Instead of a continuous function f, the lattice Boltzman distribution function is discretized so that space is divided up into a regular lattice and the velocities are represented by a finite number of displacements to neighboring sites. The displacement vectors are denoted by $\Delta t \mathbf{e}_i$, where $i = 1, \ldots, b$, Δt is the time step, and b represents the total number of displacement directions. The $\mathbf{e}_i$ have units of velocity and their magnitude is $|\mathbf{e}_i| = c$. A zero displacement vector $\mathbf{e}_0$ is included in the set to represent particles with zero velocity. The derivations described below assume that the lattices represented by the vectors $\mathbf{e}_i$ are suitably symmetric so that the tensors $\sum_{i=1}^{b} \mathbf{e}_i \mathbf{e}_i$ and $\sum_{i=1}^{b} \mathbf{e}_i \mathbf{e}_i \mathbf{e}_i \mathbf{e}_i$ are isotropic. As has been

pointed out by several authors, suitably isotropic lattices are known only in two and four dimensions [12, 13]. However, three-dimensional simulations can be recovered by using a four-dimensional lattice and making the system completely uniform along one dimension.

Two sets of distributions, f_i and F_i, are assigned to each site. The distribution f_i models the transport of mass and momentum and satisfies the two moment relations

$$\rho = \sum_{i=0}^{b} f_i \tag{2.1}$$

$$\rho \mathbf{u} = \sum_{i=1}^{b} \mathbf{e}_i f_i, \tag{2.2}$$

where ρ is the mass density and $\mathbf{u}$ is the macroscopic velocity of the fluid. The distribution F_i models the movement of internal energy around the system and satisfies the moment relation

$$\rho\epsilon = \sum_{i=0}^{b} F_i, \tag{2.3}$$

where ϵ is the specific energy per unit mass. Using a second distribution to model the energy is similar to the passive scalar approach proposed by Renda *et al.* [14] and later by Shan [8]. However, this model differs from the passive scalar approach in that changes in the energy density $\rho\epsilon$ are implicitly coupled back to the density–momentum distribution.

The distributions are updated at each time step by first performing a collision to obtain a new set of distributions and then displacing the f_i and F_i along the vector $\mathbf{e}_i$ to get a new set of distributions at each site. The collisions and displacement of the distributions are summarized by the equations of motion

$$f_i(\mathbf{r} + \Delta t\mathbf{e}_i, t + \Delta t) - f_i(\mathbf{r}, t) = -\frac{1}{\tau_\rho}\big(f_i(\mathbf{r}, t) - f_i^{eq}(\mathbf{r}, t)\big) \tag{2.4}$$

$$F_i(\mathbf{r} + \Delta t\mathbf{e}_i, t + \Delta t) - F_i(\mathbf{r}, t) = -\frac{1}{\tau_\epsilon}\big(F_i(\mathbf{r}, t) - F_i^{eq}(\mathbf{r}, t)\big), \tag{2.5}$$

where the $\mathbf{r}$ are lattice sites and t is the discrete time. Following Chen *et al.* [15], the collision operators are assumed to take the familiar BGK form [16] and are characterized for the two distributions by the dimensionless relaxation parameters τ_ρ and τ_ϵ. Because there is no explicit coupling between the equations of motion for the f_i and F_i, the total internal energy of the system is a conserved quantity, implying that there is no viscous heating in the system. For many problems of practical importance, the contribution from viscous heating is small.

To completely describe the algorithm, the equilibrium distributions f_i^{eq} and F_i^{eq} need to be specified

$$f_i^{eq} = \frac{\rho(1 - d_0)}{b} + \frac{\rho D}{bc^2}\mathbf{e}_i \cdot \mathbf{u} + \frac{\rho D(D + 2)}{2bc^4}\mathbf{u} \cdot \mathbf{e}_i\mathbf{e}_i \cdot \mathbf{u} - \frac{\rho D}{2bc^2}\mathbf{u} \cdot \mathbf{u} \tag{2.6}$$

$$f_0^{eq} = \rho d_0 - \frac{\rho}{c^2}\mathbf{u} \cdot \mathbf{u} \tag{2.7}$$

$$F_i^{eq} = \epsilon f_i^{eq} \tag{2.8}$$

$$F_0^{eq} = \epsilon f_0^{eq}. \tag{2.9}$$

The variable D is the dimension of the system and d_0 is a parameter that will be described in more detail below. The f_i^{eq} are identical to those developed for simulating a multiphase–multicomponent system [17], except that in this model d_0 is not a constant. The choice of equilibrium distribution for the F_i means that at equilibrium, the energy flux is proportional to the mass flux.

From the equilibrium distributions (2.6) and (2.7) it can be seen that the parameter d_0 controls the partition between fast and slow moving particles. If the distribution f_i can be considered to be a crude approximation to the Maxwell–Boltzmann distribution for the velocities of individual fluid particles, then as the temperature rises the velocity distribution broadens and the fraction of particles assigned to the f_i increases relative to the fraction assigned to f_0. This can only happen if d_0 decreases. Similarly, as the temperature decreases, the fraction of particles assigned to f_0 increases and d_0 increases. This suggests that d_0 is related to the local values of the density and specific energy through the temperature T. (If the specific energy ϵ and the density ρ are known at a given lattice site, then in principle the temperature and pressure can be calculated once the equation of state is specified.) As will be shown below, assuming that d_0 is related to energy and density only through the temperature turns out to be too restrictive, and better results can be obtained by treating d_0 as a general function of ϵ and ρ. By constructing a model connecting d_0 to ϵ and ρ, it is possible to incorporate the effects of thermal flow into a lattice Boltzmann algorithm consisting of the following steps:

(i) Calculate ρ, $\mathbf{u}$ and ϵ at each site using the moment relations (2.1)–(2.3).
(ii) Based on the value of ρ and ϵ, calculate the value of d_0 at each site via some as yet unspecified relation.
(iii) Evaluate f_i^{eq} and F_i^{eq} at each site and complete the collision step.
(iv) Translate the f_i and F_i.

The key feature of this algorithm is that d_0 is allowed to vary as a function of the local thermodynamic conditions at each site. This provides an implicit coupling between the two distributions f_i and F_i.

The macroscopic hydrodynamic equations generated by this model can be derived using the Chapman–Enskog multiple time scale expansion[12]. Details of this derivation are supplied in the Appendix. The continuum equations for mass, momentum, and energy that result from this analysis have the form

$$\frac{\partial}{\partial t}\rho + \partial_\alpha(\rho u_\alpha) = 0 \tag{2.10}$$

$$\frac{\partial}{\partial t}(\rho u_\alpha) + \partial_\beta(\rho u_\alpha u_\beta) = -\partial_\alpha \rho(1-d_0)\frac{c^2}{D} - \partial_\alpha \zeta \partial_\beta(\rho u_\beta) + \partial_\alpha \xi \rho u_\beta \partial_\beta \epsilon + \partial_\beta \nu \partial_\beta(\rho u_\alpha) + \partial_\beta \nu \partial_\alpha(\rho u_\beta) + \partial_\alpha \nu \partial_\beta(\rho u_\beta) \tag{2.11}$$

$$\frac{\partial}{\partial t}(\rho\epsilon) + \partial_\alpha(\rho\epsilon u_\alpha) = \partial_\alpha \kappa \partial_\alpha \epsilon. \tag{2.12}$$

The Greek indices label spatial coordinates and the Einstein convention of summing over repeated indices is used. The transport coefficients ν, ζ, ξ, and κ are defined as

$$\nu = \Delta t\left(\tau_\rho - \frac{1}{2}\right)\frac{c^2}{D+2} \tag{2.13}$$

$$\zeta = \Delta t\left(\tau_\rho - \frac{1}{2}\right)\left(\frac{c^2}{D}(1-d_0) - \frac{c^2}{D}\rho\frac{\partial d_0}{\partial \rho}\right) \tag{2.14}$$

$$\xi = \Delta t\left(\tau_\rho - \frac{1}{2}\right)\frac{c^2}{D}\frac{\partial d_0}{\partial \epsilon} \tag{2.15}$$

$$\kappa = \Delta t\left(\tau_\epsilon - \frac{1}{2}\right)\frac{c^2}{D}\rho(1-d_0). \tag{2.16}$$

The coefficient ν is the kinematic viscosity and κ is related to the thermal conductivity. Because ν and κ depend on the independent functions τ_ρ and τ_ϵ, the Prandtl number, which is proportional to the ratio of ν and κ, can be set to an arbitrary value. Comparing Eq. (2.14) with the conventional momentum equation from hydrodynamics indicates that the pressure can be identified with the quantity

$$p(\epsilon,\ \rho) = \rho(1 - d_0(\epsilon,\ \rho))\frac{c^2}{D}. \tag{2.17}$$

This can be trivially inverted to obtain d_0 as a function of ϵ and ρ. For an ideal gas, d_0 is a linear function of ϵ (or T), but for more complicated fluids d_0 depends on both ϵ and ρ.

The exact interpretation of the remaining transport coefficients ζ and ξ is not so clear. The term $-\partial_\alpha\zeta\,\partial_\beta\rho u_\beta$ can be combined with the term $\partial_\alpha\nu\partial_\beta\rho u_\beta$ to give a kinematic bulk viscosity of $\nu - \zeta$ [18]. This value of the bulk viscosity cannot be varied independently of the value of ν, because the values τ_ρ and d_0 are already constrained by the requirements that they generate the correct values of ν and the equation of state. However, for most systems the effect of the bulk viscosity is small. Both terms can be made small by adusting the time step Δt. For a given physical problem with a fixed grid, the time step can be made smaller by decreasing Δt while simultaneously increasing the lattice speed c. The relaxation parameters τ_ρ and τ_ϵ must also be adjusted so that the dissipation coefficients ν and κ remain constant. Using Eq. (2.17) for d_0, the coefficients ζ and κ can be rewritten as

$$\zeta = \Delta t\left(\tau_\rho - \frac{1}{2}\right)\frac{\partial p}{\partial \rho} \tag{2.18}$$

$$\xi = -\Delta t\left(\tau_\rho - \frac{1}{2}\right)\frac{1}{\rho}\frac{\partial p}{\partial \epsilon}. \tag{2.19}$$

Note that neither of these expressions is proportional to c^2 while ν is. Thus, if a smaller time step is used, corresponding to a larger value of c, then the terms containing ζ and ξ must become smaller relative to the viscous dissipation term. For small enough Δt, the momentum equation will reduce to

$$\begin{aligned}\frac{\partial}{\partial t}(\rho u_\alpha) + \partial_\beta(\rho u_\alpha u_\beta) = &-\partial_\alpha\rho(1-d_0)\frac{c^2}{D} + \partial_\beta\nu\partial_\beta(\rho u_\alpha)\\ &+ \partial_\beta\nu\partial_\alpha(\rho u_\beta) + \partial_\alpha\nu\partial_\beta(\rho u_\beta).\end{aligned} \tag{2.20}$$

This is just the usual momentum equation for fluid flow [11], although in this case the kinematic bulk viscosity is equal to the kinematic shear viscosity.

3. BOUNDARY CONDITIONS

The formalism described here for implementing boundary conditions is a modification of the bounce-back boundary condition, similar in spirit to the boundary conditions developed by Maier *et al.* [19] and Zou and He [20]. It assumes that all boundaries pass through a set of lattice sites that are connected to each other via the displacement vectors, $\Delta t \mathbf{e}_i$. The approach is illustrated in detail for a flat interface using the two-dimensional orthogonal lattice; the generalization to other lattices and surfaces with corners, kinks, etc. will be discussed briefly. The boundary conditions used in this study fall into two categories, either a value is specified on the boundary (Dirichlet conditions) or a flux is specified on the boundary (Neumann conditions). For fluid flow these become specified pressure (density) and specified velocity, for the energy these become specified temperature and specified energy flux.

Dirichlet boundary conditions are illustrated for the f_i by specifying a constant density at a boundary node. The method for specifying a constant energy at a boundary node using the F_i is completely analogous. The distribution f_i at the node must satisfy the condition

$$\rho_0 = \sum_{i=0}^{b} f_i, \tag{3.1}$$

where ρ_0 is the specified density. The geometry for a boundary node on a flat interface for the two-dimensional orthogonal lattice is illustrated in Fig. 1. The node at the center is the boundary node of interest and is labeled node 0, the neighboring nodes are labeled nodes 1–8. Nodes 1–3 are exterior nodes lying outside the fluid region that are used to help fix the boundary conditions at node 0, nodes 4 and 8 are two adjacent boundary nodes, and nodes 5–7 are fluid nodes that stream part of their distributions to node 0. The distributions on nodes 1–3 need to be specified after the collision step but before the streaming step. Only the parts of the distributions on nodes 1–3 that are streamed to node 0 need to be specified.

For the remaining discussion, the following notation is useful. The displacement directions are labeled by $i = 1, \ldots, 8$ and correspond to the eight neighbors of node 0 shown in Fig. 1. The distribution $f_i(j)$ refers to the distribution on node j in the direction i. The portion of the distribution on node 1 that streams towards node 0 is then $f_5(1)$. The

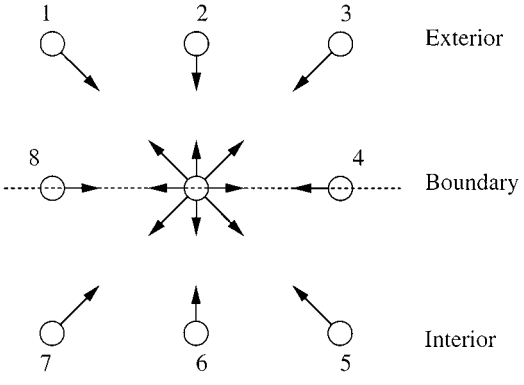

FIG. 1. Schematic diagram of boundary node for a flat boundary using the two-dimensional orthogonal lattice. The node at the center is node 0.

determination of the distributions on 1–3 consists of two steps. The first consists of pairing up each of the exterior nodes with its mirror image through node 0. Thus, node 1 is paired with node 5, node 2 is paired with node 6, and node 3 is paired with node 7. If the distribution at node 0 satisfies the boundary condition (3.1) before the streaming step, then to a first approximation the boundary condition after the streaming step is satisfied by requiring that the sum of the two opposing f_i leaving the boundary node equals the sum of the two f_i entering the boundary node. For the 1–5 pair, this is equivalent to the expression

$$f_5(1) + f_1(5) = f_5(0) + f_1(0).$$

Only the $f_5(1)$ term is unknown, so this equation can be used to find $f_5(1)$. Similar expressions can be used to find $f_6(2)$ and $f_7(3)$. If there was no net contribution to the density due to flow along the boundary, then these values for $f_5(1)$, $f_6(2)$, and $f_7(3)$ would be enough to ensure that condition (3.1) holds after the streaming step. However, because there is no guarantee that $f_8(4) + f_4(8) = f_8(0) + f_4(0)$, the distributions at nodes 1–3 must be adjusted slightly to correct for the change in density due to flow along the boundary. This correction is the second step in determining the distributions at the exterior points.

The change in the density due to flow along the boundary is labeled as

$$\Delta\rho = f_8(4) + f_4(8) - f_8(0) - f_4(0).$$

The change in density is distributed among the distributions on nodes 1–3 by an amount that is proportional to the weight that each lattice direction carries. To understand what these weights are, it is necessary to briefly consider what happens when the original four-dimensional hypercubic face-centered (HCFC) lattice is projected down into the two-dimensional orthogonal lattice. The nearest-neighbor sites of the HCFC lattice consist of all possible four-dimensional vectors with integer components whose total length is $\sqrt{2}$. This includes vectors such as $(1, 1, 0, 0)$, $(1, -1, 0, 0)$, and $(0, -1, 0, -1)$. Four of the original HCFC vectors project down to each of the axial vectors in the two-dimensional orthogonal lattice, while only one of the original HCFC vectors projects down to each of the diagonal lattice vectors. Thus, the weight w_i assigned to each of these directions is $w_1 = w_3 = w_5 = w_7 = 1$ and $w_2 = w_4 = w_6 = w_8 = 4$. Defining

$$w_{tot} = w_5 + w_6 + w_7$$

then the final expressions for $f_5(1)$, $f_6(2)$, and $f_7(3)$ are

$$\begin{aligned} f_5(1) &= f_5(0) + f_1(0) - f_1(5) - \Delta\rho w_5/w_{tot} \\ f_6(2) &= f_6(0) + f_2(0) - f_2(6) - \Delta\rho w_6/w_{tot} \\ f_7(3) &= f_7(0) + f_3(0) - f_3(7) - \Delta\rho w_7/w_{tot}. \end{aligned}$$

The method for specifying a flux-type boundary condition is similar to that for specifying a density-type boundary condition, although correcting the distributions for the flow along the boundary is more complicated. A general method for evaluating the correction due to flow along the boundary has not been worked out, but the correction for the specific case of a flat boundary is described below. The method is illustrated for the distribution f_i for the case when the velocity $\mathbf{u}$ has a value $\mathbf{u}_0$ at a surface. Prior to streaming, the momentum

density at the surface has the value

$$\rho \mathbf{u}_0 = \sum_{i=1}^{b} \mathbf{e}_i f_i. \tag{3.2}$$

Pairing the product of the f_i and $\mathbf{e}_i$ means that pairs such as the distributions at nodes 1 and 5 must satisfy an equation of the form

$$f_5(1) - f_1(5) = f_5(0) - f_1(0).$$

The difference occurs instead of the sum because $\mathbf{e}_1 = -\mathbf{e}_5$. The change in momentum at node 0 due to flow along the boundary is

$$\Delta\rho\mathbf{u} = \mathbf{e}_4 f_4(8) + \mathbf{e}_8 f_8(4) - \mathbf{e}_4 f_4(0) + \mathbf{e}_8 f_8(0). \tag{3.3}$$

There will also be a slight change in the density at node 0 after the streaming step to a new density ρ', which causes an additional change in the momentum. However, in most cases it can be assumed that this change is small and that $\rho' \sim \rho$. From Eq. (3.3), it is clear that $\Delta\rho\mathbf{u}$ is parallel to the surface. Therefore, the correction to $f_6(2)$ is zero. If the magnitude of the correction is divided evenly between $f_5(1)$ and $f_7(3)$, then this leads to the condition that $\Delta f_5(1) = -\Delta f_7(3)$. Noting that $\mathbf{e}_5 \cdot \Delta\rho\mathbf{u} = -\mathbf{e}_7 \cdot \Delta\rho\mathbf{u}$, the final expressions for the exterior distributions can be written as

$$\begin{aligned} f_5(1) &= f_5(0) - f_1(0) + f_1(5) - \mathbf{e}_5 \cdot \Delta\rho\mathbf{u}/2 \\ f_6(2) &= f_6(0) - f_2(0) + f_2(6) \\ f_7(3) &= f_7(0) - f_3(0) + f_3(7) - \mathbf{e}_7 \cdot \Delta\rho\mathbf{u}/2. \end{aligned}$$

The factor of $1/2$ arises from the particular form of the displacement vectors, $\mathbf{e}_5 = (1, -1)$ and $\mathbf{e}_7 = (-1, -1)$. The difficulty in generalizing this to an arbitrary boundary node is that there will generally be either too many or too few exterior nodes to exactly decompose the needed correction, $\Delta\rho\mathbf{u}$. It is particularly difficult to come up with a general scheme for describing a vector if the basis set is too large.

The scheme for implementing density-type boundary conditions can easily be generalized to arbitrary boundary configurations. For each boundary configuration, the set of exterior nodes is identified and paired with their mirror image through the boundary node to either a fluid or another boundary node. The unpaired fluid and boundary nodes then create a net change in the density at the boundary node that must cancelled by adding the appropriate correction to the exterior nodes. This can be done using the weighting scheme described above. For flux-type boundary conditions, the evaluation of the correction factor is complicated by the need for a general scheme for partioning a vector amongst an overdetermined nonorthogonal basis set. The development of such a scheme is currently under way.

4. RESULTS

To actually implement this algorithm, the equation of state $p(\epsilon, \rho)$ must be specified. Although the pressure for a single component fluid is more conventionally specified as a

function of temperature and density, an equivalent thermodynamic description can be given in terms of specific energy and density. For most of the simulations described below, a simple ideal gas equation of state is used. This has the form

$$p = \frac{2}{3}\rho\epsilon. \tag{4.1}$$

The temperature can be calculated from the energy via the equation

$$\epsilon = \frac{3}{2}RT, \tag{4.2}$$

where R is the ideal gas constant. For these simulations, the temperature scale was chosen so that R was equal to 1. Once the equation of state is specified, it is also possible to write down expressions for the thermal conductivity in closed form. For the ideal gas, the specific energy is solely a function of temperature, so it is possible to write

$$\kappa\nabla\epsilon = \Delta t\left(\tau_\epsilon - \frac{1}{2}\right)\frac{c^2}{D}\rho(1-d_0)\frac{3}{2}R\nabla T. \tag{4.3}$$

It follows immediately that the thermal conductivity k is

$$k = \Delta t\left(\tau_\epsilon - \frac{1}{2}\right)\frac{c^2}{D}\rho(1-d_0)\frac{3}{2}R. \tag{4.4}$$

All simulations described below were performed using the two-dimensional orthogonal lattice lattice (d2q9 in Qian *et al.*'s notation [2]) with $c = \sqrt{2}$ and $\Delta t = 1$. Because this lattice is actually a two-dimensional projection of a four-dimensional lattice, the value of D in the equilibrium distribution functions is 4. The nearest-neighbor spacing on the original lattice is $\sqrt{2}$ but after projecting down into two dimensions, the nearest-neighbor spacing is 1.

To test whether or not the lattice Boltzmann algorithm described above could model the thermal diffusion equation, a simulation of thermal conduction between two plates with a variable conductivity in the medium between the two plates was performed. For a thermal conductivity of the form,

$$k = k_0(1 + a_0T), \tag{4.5}$$

where T is the local temperature and k_0 and a_0 are adjustable parameters, an analytic solution of the thermal diffusion equation is available [21]. The temperature profile for this system is

$$T = \frac{\{(1+a_0T_1)^2 + [(1+a_0T_1)^2 - (1+a_0T_2)^2]x/L\}^{1/2} - 1}{a_0}, \tag{4.6}$$

where L is the distance between the two plates and x is the position between the two plates. The location of plate 1 is at $x = 0$ and the location of plate 2 is at $x = L$. The temperatures T_1 and T_2 are the temperatures at plates 1 and 2, respectively. The local value of τ_ϵ was chosen by first determining the local value of k and then inverting Eq. (4.4) to get τ_ϵ. The simulations were performed on a 53×5 node lattice. The long axis of the simulation cell was perpendicular to the surface of the two plates and the system was completely uniform along

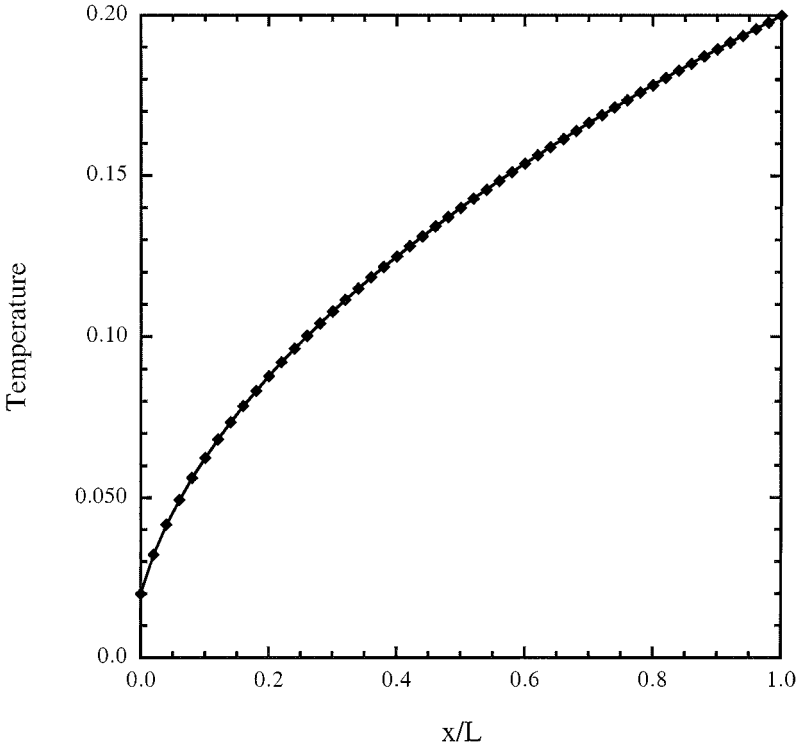

FIG. 2. Plot of temperature as a function of position for nonlinear conduction problem. The symbols are calculated from the lattice Boltzmann simulation, the solid line is the analytic result.

the short axis (the system is actually one-dimensional and a two-dimensional simulation cell was used only for convenience). Two of the nodes at the ends of the long axis were used as exterior nodes to establish boundary conditions at the wall and periodic boundary conditions were applied to the short axis. The average density in the cell was set at $\bar{\rho} = 0.1$ and the temperatures at the surface of the plates were $T_1 = 0.02$ and $T_2 = 0.2$. Both the parameters a_0 and k_0 were set to 100. The temperature profile calculated from the simulation after equilibrating to a stationary state is shown in Fig. 2 and is compared to the analytic solution (4.6). The curves are indistinguishable from each other. This is not surprising, because the hydrodynamic analysis shows that in the absence of any fluid motion ($\mathbf{u} = \mathbf{0}$ everywhere) the hydrodynamic equations for this model reduce down to the thermal diffusion equation exactly.

To test the lattice Boltzmann algorithm for a system with a finite fluid velocity, simulations of entry length behavior in flow down a channel were performed. The phenomena being studied is the distance down the channel required for the fluid to reequilibrate to a new temperature if the wall temperatures are abruptly changed from a temperature T_0 to a new temperature T_1. A 200×43 node lattice was used for these simulations. The long axis of the simulation cell corresponds to the channel axis and the shorter axis is perpendicular to the channel. Two of the lattice nodes in the direction normal to the flow where used as exterior nodes to establish boundary conditions on each wall. The simulations were allowed to run until a steady-state was achieved. For the entry length simulations described below, the velocities were less than 0.34. This range corresponds to Reynolds numbers less than

200, which is low enough that the flow could be considered incompressible. At the entrance of the channel the temperature distribution is uniform, with a value T_0, and the velocity profile is parabolic. At the channel exit the pressure was set equal to a constant and the energy gradient was set equal to zero. Because the system is slightly compressible, the fluid was allowed to flow down a short stretch of channel (20 lattice units) with the walls at temperature T_0 in order for the fluid profile to relax completely. The wall temperature was then abruptly changed to a new temperature T_1. The point at which the temperature change occurred was considered the origin for the entry length behavior. Analytic solutions for the Nusselt number Nu as a function of position have been obtained for this problem and can be used to compare with the results of simulations [22]. (These solutions assume that the fluid is incompressible, that axial diffusion is negligable, and that the parabolic flow profile is uniform down the length of the channel.)

The requirement that axial diffusion is negligable is equivalent to the condition that the product of the Reynolds number Re and the Prandtl number be greater than about 100. This product is equal to the Peclet number, Pe. Simulations were run for a values of Pe equal to 200 and 400. Two simulations at values of the Prandtl number equal to 1 and 2 were run at flow conditions corresponding to a value of the Reynolds number of 200. The values of τ_ρ and τ_ϵ for these simulations were $\tau_\rho = 0.77$ and $\tau_\epsilon = 0.75$ for $\mathrm{Pr} = 1$ and $\tau_\rho = 0.68$ and $\tau_\epsilon = 1.0$ for $\mathrm{Pr} = 2$. The temperature T_1 was set at 0.101 and T_2 was set at 0.100. The Nusselt number is plotted in Fig. 3 as a function of the reduced position $x^+ = (x/L)/\mathrm{Pe}$,

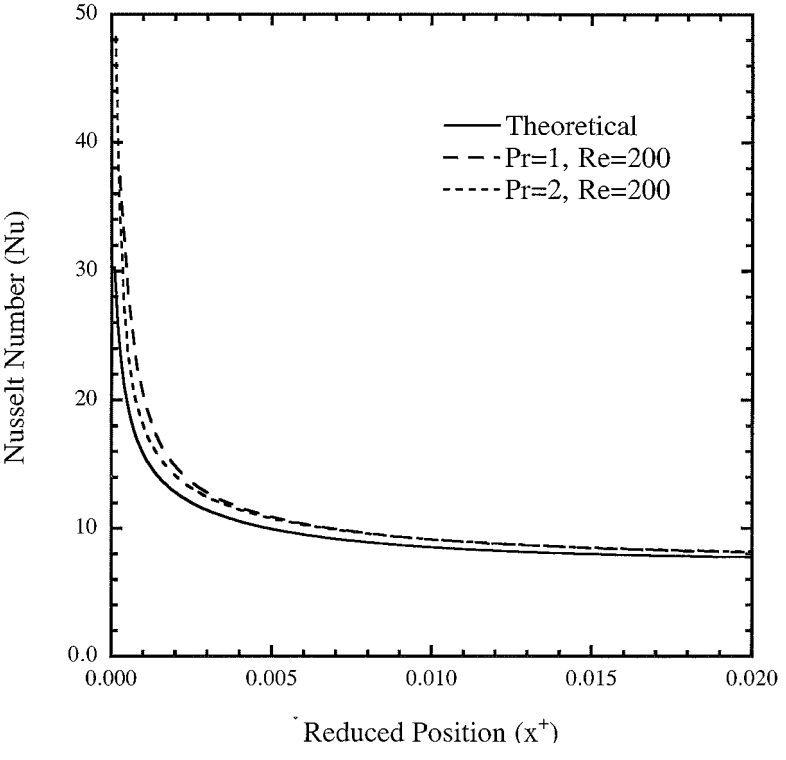

FIG. 3. Plot of Nusselt number, Nu, as a function of reduced position x^+ from the temperature jump. The solid line is the analytic result, the dashed line is for a Prandtl number of 1 and the dotted line is for a Prandtl number of 2.

where L is the channel half-width and x is the position from the temperature jump. The analytic solution is also included in the figure. When plotted in this way, the Nusselt number is a universal function of x^+, so both simulations should lie on the same curve. All systems investigated, which included a number of values of Pr and Re not reported here, showed the correct asymtotic behavior at large x^+, and approached the limiting Nusselt number of 7.54. Figure 3 focuses on the region near the temperature jump and exhibits quite good agreement between the simulations and the analytic result. The analytic result is singular at the origin, while the simulated curve, which in some sense represents the flux averaged over a node spacing, is necessarily finite. This probably accounts for most of the deviation between the analytic results and the lattice Boltzmann simulations near the origin. Some of the difference may also be due to a small amount of axial diffusion in the simulations that is not accounted for in the analytic result. As the Peclet number increases, the discrepancy decreases.

Finally, simulations of Rayleigh–Bénard flow were performed to determine if the algorithm could correctly model the effects of compressibility. Following Shan [8], the growth rate of small perturbations was calculated as a function of the Rayleigh number, Ra, and extrapolated back to zero growth rate to determine the critical Ralyeigh number. This could then be compared with analytic results. The simulations were performed on a 53×100 node lattice that was periodic along the long axis. One node at each of the ends of the short axis was used as an exterior node to impose boundary conditions at the wall. A periodic disturbance in this system corresponds to a reduced wave number of 3.142, which is only slightly larger than the critical wavenumber, $k_c = 3.117$ [23]. Gravity was introduced into the simulation using a method similar to the one recently proposed by Buick and Greated [24]. This involves modifying the distribution f_i at $\mathbf{r}$ to

$$f_i' = f_i + \frac{\bar{\rho} D}{bc^2} \mathbf{e}_i \cdot \mathbf{g}, \tag{4.7}$$

where $\bar{\rho}$ is equal to $(\rho(\mathbf{r}) + \rho(\mathbf{r} + \Delta t \mathbf{e}_i))/2$ and $\mathbf{g}$ is the gravity vector. The average density in this system was $\rho = 1.0$, the temperatures of the lower and upper plates were $T = 0.22$ and $T = 0.18$, respectively, and the magnitude of gravity was $|\mathbf{g}| = 0.0001$. The energy relaxation parameter τ_ϵ was chosen so that $k = 0.01$ everywhere, and the momentum relaxation parameter τ_ρ was varied in the range 0.88 to 0.92 to obtain different values of the Rayleigh number.

Because the fluid is compressible, it is extremely difficult to set up an initial condition that will grow smoothly enough that an unambiguous growth exponent can be extracted from it. The initial conditions were prepared by first starting with a system that was completely uniform in the horizontal direction and allowing it to equilibrate under the influence of the temperature gradient and gravity for 10,000 time steps. The uniformity of the initial condition in the horizontal direction prevented the growth of an instability during the equilibration phase. After equilibration, a perturbation of the form

$$\delta\rho = \Delta\rho \cos(2\pi x / W) \sin(\pi y / L) \tag{4.8}$$

was added to the density. The width of the periodic simulation cell was W and x was the position along the direction parallel to the surfaces. The separation of the upper and lower surfaces was L and y was the height from the lower surface. The temperature was simultaneously adjusted so that the pressure at each point was the same as the pressure before the

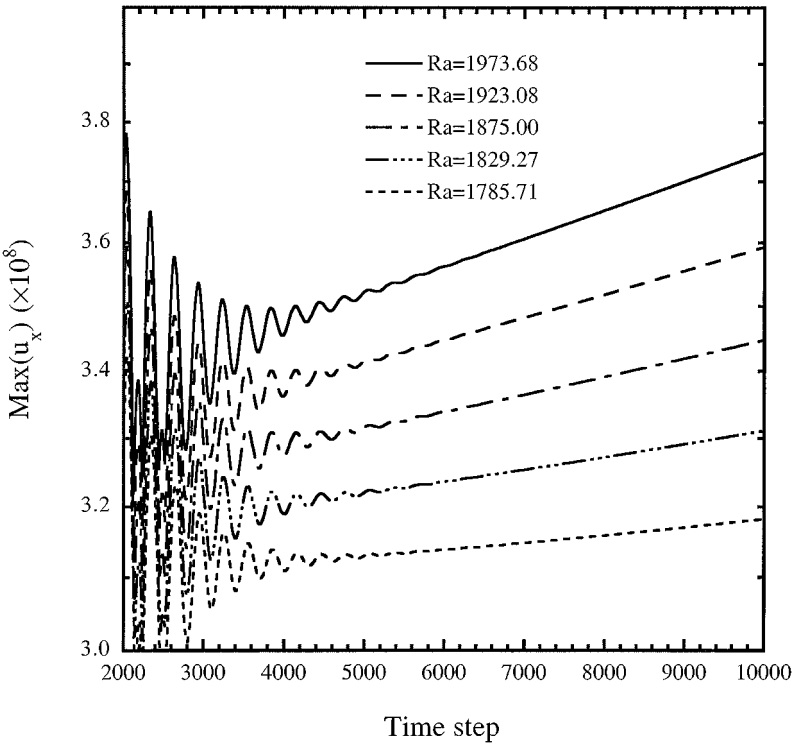

FIG. 4. Plots of max(u_x) as a function of time step for different values of the Rayleigh number, Ra. Plots are from simulations using ideal gas thermodynamics.

density perturbation was applied. The use of this particular form of the perturbation minimized oscillations of the fluid after the perturbation was applied that tended to mask the growth rate of the perturbation. The maximum velocity in the x direction was monitored as a function of time. After an initial period characterized by some damped oscillations superimposed on the growth curve, the maximum value of u_x grew exponentially as $u_x \sim \exp(\omega t)$, and the growth rate ω could be extracted from fits of max(u_x) versus time. The first 6000 steps after the application of the perturbation were discarded and the values of ω were obtained from the values of max(u_x) between 6000 and 10,000 steps after the perturbation. The value of the critical Rayleigh number could then be determined by finding the value of Ra for which $\omega = 0$. Plots of max(u_x) as a function of time are shown for several values of Ra in Fig. 4. The oscillations at early times are quite evident, but the plots are smooth in the regime from 6000 to 10,000 time steps. A fit to these curves was used to obtain ω for different values of Ra and a plot of ω as a function of Ra is shown in Fig. 5. The value of the critical Rayleigh number, Ra_c, was calculated by extrapolating the curve down to $\omega = 0$. Because the function ω(Ra) is slightly nonlinear, only the three points closest to the value $\omega = 0$ were used in the extrapolation. This gave a value of $\mathrm{Ra}_c = 1718$ which compares very favorably with the analytic value of $\mathrm{Ra}_c = 1707.76$ [23].

The original stability analysis used to calculate Ra_c assumed ideal gas thermodynamics for the fluid. To find out what effect using a more realistic model of the fluid has on the evaluation of the critical Rayleigh number, the simulations described above were repeated using a Van der Waals fluid for the equation of state. The pressure and energy for the Van

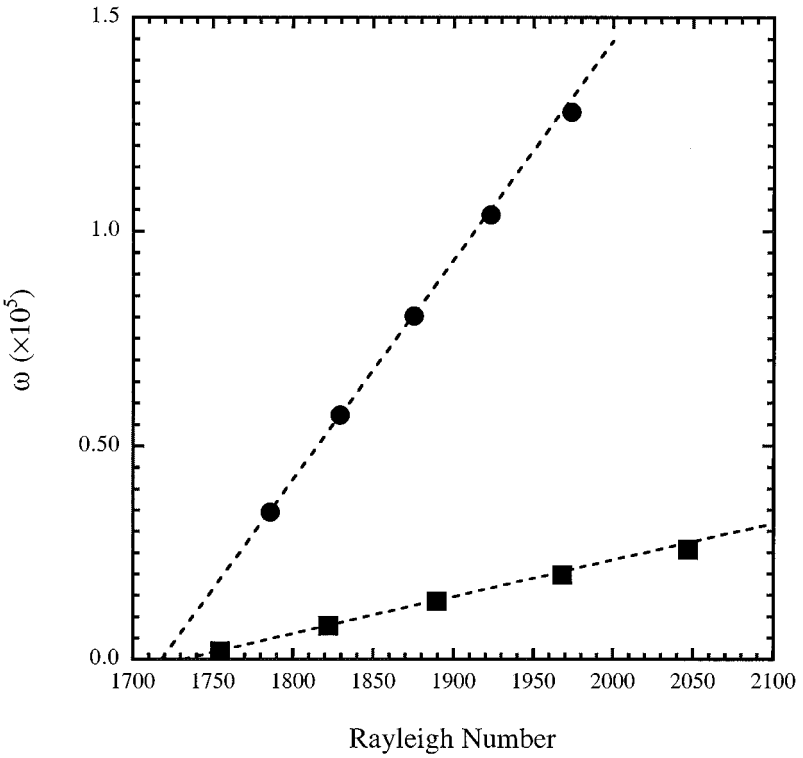

FIG. 5. Plot of the perturbation growth rate ω as a function of Rayleigh number, Ra. The linear fit to the three points closest to $\omega = 0$ is also included. The circles are for simulations using ideal gas thermodynamics, the squares are for simulations using the Van der Waals fluid.

der Waals fluid are given by [25, 26]

$$p = \frac{\rho RT}{1 - b\rho} - a\rho^2 \tag{4.9}$$

$$\epsilon = \frac{3}{2} RT - a\rho, \tag{4.10}$$

where a and b are constants that are different for each fluid. These were set to the values $a = 9/8$ and $b = 1/3$ (the critical temperature and density are both unity for this choice). The contribution to the heat flux from density gradients was assumed to be small, and Eq. (4.4) was still used to evaluate τ_ϵ. The temperatures of the lower and upper plates were set at 0.9 and 0.6 and the average density was chosen to be 2.2. This corresponds to a liquid region of the phase diagram. For this system, different Rayleigh numbers were obtained by varying k in the range 0.012 to 0.014. The remaining parameters were the same as for the simulations of the ideal gas. The results are included in Fig. 5. The values of ω as a function of Ra vary much more slowly for the Van der Waals liquid than for the ideal gas, but the value of the intercept only increases slightly. The intercept obtained from the simulations is 1732, which is still quite close to the predicted value of 1707.76.

5. CONCLUSIONS

A new lattice Boltzmann algorithm for simulating thermal flows in the absense of significant heating due to viscous dissipation has been presented. The algorithm is based on the

introduction of a second distribution to model the flow of internal energy through the system. This algorithm has the advantages that it only requires two speeds to simulate thermal flow, so all the lattices that have been adapted for simulating incompressible Navier–Stokes flow using the traditional lattice Boltzmann model can be used for simulating thermal flows. Unlike algorithms based on treating the internal energy as a higher order moment of the mass-momentum distribution, the two-distribution algorithm can be used with an arbitrary equation of state. Previous algorithms for simulating thermal flow appear to be restricted to an ideal gas equation of state. An additional feature of this lattice Boltzmann model is that it can simulate a range of Prandtl numbers while still retaining the simple BGK form for the collision operators.

The fact that the equation of state can be specified independently of the lattice speed c also means that it is possible to change the time step Δt without altering the rest of the problem (although it is necessary to simultaneously adjust τ_ρ and τ_ϵ so that the transport coefficients ν and κ remain the same). Increasing c results in a corresponding decrease in Δt. This can be used to obtain results for problems that are unstable using larger values of Δt. The algorithm described here was able to obtain results using smaller values of the time step for problems that were characterized as unstable [4, 14] using the original thermal algorithm of Alexander *et al.* [3].

The hydrodynamic behavior of the model has been determined and reproduces the conventional hydrodynamic equations for thermal flow in the absence of viscous dissipation, with the exception of two extra terms that appear in the momentum equation. However, these terms vanish in the limit of small time step. The hydrodynamic analysis also provides closed-form expressions that relate the parameters of the lattice Boltzmann model to the macroscopic transport coefficients and the equation of state.

The algorithm was tested on several hydrodynamic problems for which analytic results are available. These included nonlinear thermal conductivion between two plates, entry-length behavior for flow in a channel, and a calculation of the critical Rayleigh number for Rayleigh–Bénard convection between two plates. The simulations were in quantitative agreement with the analytic results for all cases. The agreement with theory is particularly encouraging in the case of the evaluation of the critical Rayleigh number, since this was calculated entirely from transients. This suggests that the effect of the extra terms identified in the momentum equation is small. The results for the Rayleigh-Bénard instability also indicate that the thermal lattice Boltzmann algorithm contains all the necessary physics for simulating natural convection.

The algorithm can be extended in a number of directions. Two areas that are currently being pursued are correcting the thermal diffusion term so that the heat flux is proportional to the gradient of the temperature for all fluids, not just those with ideal gas or hard sphere thermodynamics, and combining the thermal model with a two-phase model so that it will be possible to model the dynamics of thermally driven phase changes. Other areas for future work include the inclusion of additional source terms in the energy equation to model the conversion of mechanical energy to internal energy via pressure-volume work and viscous dissipation.

APPENDIX

This appendix will describe in detail the derivation of the hydrodynamic equations generated by the lattice Boltzmann model described in the text. The derivation is based on a

Chapman–Enskog multiple time scale expansion [12] of the equations of motion (2.4) and (2.5). The distributions f_i and F_i are assumed to have an expansion in a small parameter λ of the form

$$f_i = f_i^{eq} + \lambda f_i^{(1)} + \lambda^2 f_i^{(2)} + \mathcal{O}(\lambda^3) \tag{A.1}$$

$$F_i = F_i^{eq} + \lambda F_i^{(1)} + \lambda^2 F_i^{(2)} + \mathcal{O}(\lambda^3). \tag{A.2}$$

The dimensionless variable λ can be thought of as being the inverse of the time scale for propagating hydrodynamic modes such as pressure waves. Diffusive modes, such as shear relaxation, decay on a timescale of order λ^{-2}. The hydrodynamic length scale is of the order λ^{-1}.

The Chapman–Enskog expansion begins by expanding the equations of motion (2.4) and (2.5) to second order about $\mathbf{r}$ and t. This gives

$$\begin{aligned}\Delta t\frac{\partial}{\partial t} f_i + \Delta t\mathbf{e}_i\cdot\nabla f_i + \frac{1}{2}\Delta t^2\frac{\partial^2}{\partial t^2} f_i + \Delta t^2\mathbf{e}_i\cdot\nabla\frac{\partial}{\partial t} f_i \\ + \frac{1}{2}\Delta t^2\mathbf{e}_i\mathbf{e}_i:\nabla\nabla f_i = -\frac{1}{\tau_\rho}\left(f_i - f_i^{eq}\right).\end{aligned} \tag{A.3}$$

$$\begin{aligned}\Delta t\frac{\partial}{\partial t} F_i + \Delta t\mathbf{e}_i\cdot\nabla F_i + \frac{1}{2}\Delta t^2\frac{\partial^2}{\partial t^2} F_i + \Delta t^2\mathbf{e}_i\cdot\nabla\frac{\partial}{\partial t} F_i \\ + \frac{1}{2}\Delta t^2\mathbf{e}_i\mathbf{e}_i:\nabla\nabla F_i = -\frac{1}{\tau_\epsilon}\left(F_i - F_i^{eq}\right).\end{aligned} \tag{A.4}$$

The next step is to replace the variables $\mathbf{r}$ and t by the variables $\mathbf{r}_1$, t_1, and t_2 where $\mathbf{r} = \lambda\mathbf{r}_1$, $t_1 = \lambda t$, and $t_2 = \lambda^2 t$. This is equivalent to replacing the derivatives with respect to $\mathbf{r}$ and t by the expressions

$$\begin{aligned}\frac{\partial}{\partial t} &= \lambda\frac{\partial}{\partial t_1} + \lambda^2\frac{\partial}{\partial t_2} \\ \nabla &= \lambda\nabla_1.\end{aligned}$$

Using these relations in Eqs. (A.3) and (A.4), along with the expansions (A.1) and (A.2), and equating the coefficients of λ up to order λ^2 leads to the following set of four coupled equations

$$\frac{\partial}{\partial t_1} f_i^{eq} + \mathbf{e}_i\cdot\nabla_1 f_i^{eq} = -\frac{1}{\Delta t\tau_\rho} f_i^{(1)} \tag{A.5}$$

$$\begin{aligned}\frac{\partial}{\partial t_2} f_i^{eq} + \frac{\partial}{\partial t_1} f_i^{(1)} + \mathbf{e}_i\cdot\nabla_1 f_i^{(1)} + \frac{1}{2}\Delta t\frac{\partial^2}{\partial t_1^2} f_i^{eq} + \Delta t\mathbf{e}_i\cdot\nabla_1\frac{\partial}{\partial t_1} f_i^{eq} \\ + \frac{1}{2}\Delta t\mathbf{e}_i\mathbf{e}_i:\nabla_1\nabla_1 f_i^{eq} = -\frac{1}{\Delta t\tau_\rho} f_i^{(2)}\end{aligned} \tag{A.6}$$

$$\frac{\partial}{\partial t_1} F_i^{eq} + \mathbf{e}_i\cdot\nabla_1 F_i^{eq} = -\frac{1}{\Delta t\tau_\epsilon} F_i^{(1)} \tag{A.7}$$

$$\begin{aligned}\frac{\partial}{\partial t_2} F_i^{eq} + \frac{\partial}{\partial t_1} F_i^{(1)} + \mathbf{e}_i\cdot\nabla_1 F_i^{(1)} + \frac{1}{2}\Delta t\frac{\partial^2}{\partial t_1^2} F_i^{eq} + \Delta t\mathbf{e}_i\cdot\nabla_1\frac{\partial}{\partial t_1} F_i^{eq} \\ + \frac{1}{2}\Delta t\mathbf{e}_i\mathbf{e}_i:\nabla_1\nabla_1 F_i^{eq} = -\frac{1}{\Delta t\tau_\rho} F_i^{(2)}.\end{aligned} \tag{A.8}$$

The remaining step is to take moments of Eqs. (A.5)–(A.8) to generate the equations of motion for the macroscopic continuum variables ρ, $\mathbf{u}$, and ϵ. The equilibrium distribution functions already satisfy the moment relations (2.1)–(2.3). This can be verified by direct calculation and using the lattice vector relation [12]

$$\sum_{i=1}^{b} e_{i\alpha} e_{i\beta} = \frac{bc^2}{D} \delta_{\alpha\beta}.$$

Use is also made of the property that sums over odd numbered products of lattice vectors vanish. Because the equilibrium distributions satisfy Eqs. (2.1)–(2.3), the following moments must vanish

$$\sum_{i=0}^{b} f_i^{(n)} = 0 \tag{A.9}$$

$$\sum_{i=1}^{b} \mathbf{e}_i f_i^{(n)} = \mathbf{0} \tag{A.10}$$

$$\sum_{i=0}^{b} F_i^{(n)} = 0 \tag{A.11}$$

whenever $n \geq 1$.

Summing the first-order equations (A.5) and (A.7) over i and making extensive use of the moment relations (2.1)–(2.3) and (A.9)–(A.11) gives the first-order equations for the density and energy

$$\frac{\partial}{\partial t_1} \rho + \partial_{1\alpha}(\rho u_\alpha) = 0 \tag{A.12}$$

$$\frac{\partial}{\partial t_1}(\rho\epsilon) + \partial_{1\alpha}(\rho\epsilon u_\alpha) = 0. \tag{A.13}$$

$$\tag{A.14}$$

Multiplying Eq. (A.5) by the lattice vectors $\mathbf{e}_i$ and summing over i gives the first-order equation for the momentum

$$\frac{\partial}{\partial t_1}(\rho u_\alpha) + \partial_{1\beta}(\rho u_\alpha u_\beta) = -\partial_{1\alpha}\rho(1 - d_0)\frac{c^2}{D}. \tag{A.15}$$

Equation (A.15) follows directly from the moment relations and the definition of f_i^{eq}. It also makes use of the identity

$$\sum_{i=1}^{b} e_{i\alpha} e_{i\beta} e_{i\gamma} e_{i\delta} = \frac{bc^4}{D(D+2)}(\delta_{\alpha\beta}\delta_{\gamma\delta} + \delta_{\alpha\gamma}\delta_{\beta\delta} + \delta_{\alpha\delta}\delta_{\beta\gamma}),$$

which holds for any lattice with suitable isotropy properties [12].

The second-order equations are more complicated. Summing Eq. (A.6) over i gives

$$\frac{\partial}{\partial t_2}\rho + \frac{1}{2}\Delta t \frac{\partial}{\partial t_1}\left[\frac{\partial}{\partial t_1}\sum_{i=0}^{b} f_i^{eq} + \partial_{1\alpha}\sum_{i=1}^{b} e_{i\alpha} f_i^{eq}\right] + \frac{1}{2}\Delta t \partial_{1\alpha}\left[\frac{\partial}{\partial t_1}\sum_{i=0}^{b} e_{i\alpha} f_i^{eq} + \partial_{1\alpha}\sum_{i=0}^{b} e_{i\alpha}e_{i\beta} f_i^{eq}\right] = 0. \tag{A.16}$$

The first-order equations can be used to show that the bracketed terms in (A.16) vanish and the second order equation for the density becomes

$$\frac{\partial}{\partial t_2}\rho = 0. \tag{A.17}$$

Similar manipulations can be used to reduce the second-order momentum equation to

$$\frac{\partial}{\partial t_2}(\rho u_\alpha) + \partial_{1\alpha}\sum_{i=1}^{b} e_{i\alpha}e_{i\beta} f_i^{(1)} + \frac{1}{2}\Delta t \partial_{1\beta}\left[\frac{\partial}{\partial t_1}\sum_{i=1}^{b} e_{i\alpha}e_{i\beta} f_i^{eq} + \partial_{1\gamma}\sum_{i=1}^{b} e_{i\alpha}e_{i\beta}e_{i\gamma} f_i^{eq}\right] = 0. \tag{A.18}$$

The term proportional to $f_i^{(1)}$ cannnot be eliminated using any of the moment relations (A.9)–(A.11). However, it is possible to solve Eq. (A.5) for $f_i^{(1)}$ in terms of the f_i^{eq} and use the result in Eq. (A.18) to get

$$\frac{\partial}{\partial t_2}(\rho u_\alpha) - \partial_{1\beta}\Delta t\left(\tau_\rho - \frac{1}{2}\right)\left[\frac{\partial}{\partial t_1}\sum_{i=1}^{b} e_{i\alpha}e_{i\beta} f_i^{eq} + \partial_{1\gamma}\sum_{i=1}^{b} e_{i\alpha}e_{i\beta}e_{i\gamma} f_i^{eq}\right] = 0. \tag{A.19}$$

Note that τ_ρ and τ_ϵ are assumed to depend on space and time so that they can eventually be made functions of the local temperature and density. Using the explicit definitions of the f_i^{eq} and neglecting any terms of order u^2 or higher leads to an equation entirely in terms of the macroscopic continuum variables

$$\frac{\partial}{\partial t_2}(\rho u_\alpha) - \partial_{1\beta}\Delta t\left(\tau_\rho - \frac{1}{2}\right)\left[\frac{\partial}{\partial t_1}\rho(1-d_0)\frac{c^2}{D}\delta_{\alpha\beta} + \partial_{1\gamma}\rho\frac{c^2}{D+2}(\delta_{\alpha\beta}\delta_{\gamma\delta} + \delta_{\alpha\gamma}\delta_{\beta\delta} + \delta_{\alpha\delta}\delta_{\beta\gamma})u_\delta\right] = 0. \tag{A.20}$$

The remaining step is to eliminate the derivative with respect to t_1. This can be done by using the first-order equations to replace all derivatives with respect to t_1 with gradients with respect to $\mathbf{r}_1$. The t_1 derivative in Eq. (A.20) becomes

$$\frac{\partial}{\partial t_1}\rho(1-d_0)\frac{c^2}{D} = -(1-d_0)\frac{c^2}{D}\partial_{1\alpha}(\rho u_\alpha) + \rho\frac{c^2}{D}\frac{\partial d_0}{\partial \rho}\partial_{1\alpha}(\rho u_\alpha) + \rho\frac{c^2}{D}\frac{\partial d_0}{\partial \epsilon}u_\alpha\partial_{1\alpha}\epsilon. \tag{A.21}$$

Combining (A.20) and (A.21) gives the final form for the second-order momentum

equation

$$\frac{\partial}{\partial t_2}(\rho u_\alpha) + \partial_{1\alpha}\Delta t\left(\tau_\rho - \frac{1}{2}\right)\left[(1-d_0)\frac{c^2}{D} - \rho\frac{c^2}{D}\frac{\partial d_0}{\partial \rho}\right]\partial_{1\beta}(\rho u_\beta)$$
$$- \partial_{1\alpha}\Delta t\left(\tau_\rho - \frac{1}{2}\right)\frac{c^2}{D}\frac{\partial d_0}{\partial \epsilon}\rho u_\beta \partial_{1\beta}\epsilon - \partial_{1\alpha}\Delta t\left(\tau_\rho - \frac{1}{2}\right)\frac{c^2}{D+2}\partial_{1\beta}(\rho u_\beta)$$
$$- \partial_{1\beta}\Delta t\left(\tau_\rho - \frac{1}{2}\right)\frac{c^2}{D+2}\partial_{1\alpha}(\rho u_\beta) - \partial_{1\beta}\Delta t\left(\tau_\rho - \frac{1}{2}\right)\frac{c^2}{D+2}\partial_{1\beta}(\rho u_\alpha) = 0. \quad \text{(A.22)}$$

The second-order energy equation can be obtained using methods very similar to those used to evaluate the second order momentum equation. Summing Eq. (A.8) over i leads to

$$\frac{\partial}{\partial t_2}(\rho\epsilon) - \partial_{1\alpha}\Delta t\left(\tau_\epsilon - \frac{1}{2}\right)\left[\frac{\partial}{\partial t_1}\rho\epsilon u_\alpha + \partial_{1\alpha}\rho\epsilon(1-d_0)\frac{c^2}{D}\right] = 0. \quad \text{(A.23)}$$

All terms of order u^2 have been dropped. The first-order equations can be used to eliminate the derivative with respect to t_1. After again dropping all terms of order u^2, the final result for the second-order energy equation is

$$\frac{\partial}{\partial t_2}(\rho\epsilon) - \partial_{1\alpha}\Delta t\left(\tau_\epsilon - \frac{1}{2}\right)\rho(1-d_0)\frac{c^2}{D}\partial_{1\alpha}\epsilon = 0. \quad \text{(A.24)}$$

Combining the first- and second-order equations and eliminating the variables t_1, t_2, and $\mathbf{r}_1$ in favor of t and $\mathbf{r}$ leads to the hydrodynamic equations (2.10)–(2.12).

REFERENCES

1. H. Chen, S. Chen, and W. H. Matthaeus, Recovery of the Navier–Stokes equations using a lattice-gas Boltzmann method, *Phys. Rev. A* **45**, R5339 (1992).
2. Y. H. Qian, D. d'Humières, and P. Lallemand, Lattice BGK models for Navier–Stokes equation, *Europhys. Lett.* **17**, 479 (1992).
3. F. J. Alexander, S. Chen, and J. D. Sterling, Lattice Boltzmann thermohydrodynamics, *Phys. Rev. E.* **47**, R2249 (1993).
4. G. R. McNamara, A. L. Garcia, and B. J. Alder, Stabilization of thermal lattice Boltzmann models, *J. Stat. Phys.* **81**, 395 (1995).
5. G. McNamara and B. Alder, Analysis of the lattice Boltzmann treatment of hydrodynamics, *Physica A* **194**, 218 (1993).
6. M. Soe, G. Valhala, P. Pavlo, L. Valhala, and H. Chen, Thermal lattice Boltzmann simulations of variable Prandtl number turbulent flows, *Phys. Rev. E* **57**, 4227 (1998).
7. F. Massaioli, R. Benzi, and S. Succi, Exponential tails in two-dimensional Rayleigh–Bénard convection, *Europhys. Lett.* **21**, 305 (1993).
8. X. Shan, Simulation of Rayleigh–Bénard convection using a lattice Boltzmann method, *Phys. Rev. E* **55**, 2780 (1997).
9. X. He, S. Chen, and G. Doolen, A novel thermal model for the lattice Boltzmann method in incompressible limit, *J. Comput. Phys.* **146**, 282 (1998).
10. D. Rector, J. Cuta, and B. Palmer, Lattice-Boltzmann simulation code development for micro-fluidic systems, *Process Miniaturization: 2nd International Conference on Microreaction Technology, New Orleans, 1998*, p. 272 (AICHE, New York, 1998). [There is a mistake in the momentum equation in this paper (Equation 11) due to incorrectly transcribing from Einstein to vector notation.]

11. L. D. Landau and E. M. Lifshitz, *Fluid Mechanics* (Pergamon Press, New York, 1959).
12. U. Frisch, D. d'Humières, B. Hasslacher, P. Lallemand, Y. Pomeau, and J.-P. Rivet, Lattice gas hydrodynamics in two and three dimensions, *Complex Systems* **1**, 649 (1987).
13. S. Wolfram, Cellular automaton fluids 1: Basic theory. *J. Stat. Phys.* **45**, 471 (1986).
14. A. Renda, G. Bella, S. Succi, and I. V. Karlin, Thermohydrodynamic lattice BGK schemes with non-perturbative equilibria, *Europhys. Lett.* **41**, 279 (1998).
15. S. Chen, H. Chen, D. Martinez, and W. Matthaeus, Lattice Boltzmann model for simulation of magnetohydrodynamics, *Phys. Rev. Lett.* **67**, 3776 (1991).
16. P. L. Bhatnagar, E. P. Gross, and M. Krook, A model for collision processes in gases. I. Small amplitude processes in charged and neutral one-component systems, *Phys. Rev.* **94**, 511 (1954).
17. X. Shan and H. Chen, Lattice Boltzmann model for simulating flows with multiple phases and components, *Phys. Rev. E.* **47**, 1815 (1993).
18. W. Hughes and E. Gaylord, *Basic Equations of Engineering Science* (McGraw-Hill, New York, 1964).
19. R. Maier, R. Bernard, and D. Grunau, Boundary conditions for the lattice Boltzmann method, *Phys. Fluids* **8**, 1788 (1996).
20. Q. Zou and X. He, On pressure and velocity boundary conditions for the lattice Boltzmann BGK model, *Phys. Fluids* **9**, 1591 (1997).
21. W. Rohsenow and J. Hartnett (Eds.), *Handbook of Heat Transfer* (McGraw-Hill, New York, 1973).
22. W. M. Kays, *Convective Heat and Mass Transfer* (McGraw-Hill, New York, 1966).
23. S. Chandresekhar, *Hydrodynamic and Hydromagnetic Stability* (Clarendon Press, Oxford, 1961).
24. J. Buick and C. Greated, Lattice Boltzmann modeling of interfacial gravity waves, *Phys. Fluids* **10**, 1490 (1998).
25. D. A. McQuarrie, *Statistical Mechanics*, (Harper & Row, New York, 1973).
26. K. Denbigh, *The Principles of Chemical Equilibrium* (Cambridge University Press, Cambridge, 1981).